Development of a population balance modelling for predicting bubble size distribution dynamics

Diogo Alexandre dos Santos Abreu
diogo.santos.abreu@tecnico.ulisboa.pt

Instituto Superior Técnico, Lisboa, Portugal

November 2018

Abstract

Aeration is the most energy demanding process in wastewater treatment plants, thus the optimisation of its efficiency has been identified as one of the most crucial endeavours in the field of wastewater engineering. Mathematical modelling of oxygen transfer is a possible solution to this problem, since it enables the comprehension of the underlying physical phenomena involved in this complex process. Although bubble size distribution (BSD) has been pinpointed as one of the key factors in the estimation of oxygen transfer, most state-of-the-art modelling methodologies fail to consider the impact of this parameter. This thesis aims to fill the knowledge gap associated with the influence of BSD on oxygen transfer. To achieve this, a mathematical model that predicts BSD dynamics was developed. The model is based on the population balance modelling (PBM) framework and on a coalescence model. This strategy was applied to a lab scale bubble column to assess its predictive capability. Results show that the model developed is able to accurately predict experimental observations, proving that it can be a valuable tool in estimating BSD dynamics. Therefore, this work is a first step towards the refinement of current oxygen transfer models and, as such, it paves the way for the reduction of energy consumption in wastewater treatment plants.
Keywords: Aeration; Coalescence; Energy efficiency; Oxygen transfer; Wastewater treatment

1. Introduction

Water is an essential resource for human life, ecosystems, and the industry (Maitland, 1990). In many locations, the amount of available fresh water to fulfil human needs has become insufficient (Metcalf and Eddy, 2003). This condition will tend to worsen throughout the years, since the Earth's population will keep rising and the amount of available fresh water is limited (Maitland, 1990). Furthermore, once fresh water is used by an organism or in a human activity, it usually becomes polluted, which makes it unusable and a hazard to public health and the environment. Therefore, its treatment and potential reuse is of the utmost importance. To accomplish this objective, wastewater engineering is an indispensable field (Metcalf and Eddy, 2003).

The conventional wastewater treatment scheme is composed of four steps: (1) pre-treatment, (2) primary treatment, (3) secondary treatment with nutrient removal, and (4) tertiary treatment (Metcalf and Eddy, 2003; Mihelcic and Zimmerman, 2010). The third stage of this scheme includes a biological treatment: a key activity to the overall process. The main objective of this step is the transformation of dissolved and particulate biodegradable constituents (organic matter) into acceptable end products and removal of nutrients (such as Nitrogen and Phosphorous) using microorganisms, principally bacteria. One of the most commonly used biological processes in wastewater treatment is the activated sludge (AS) process (Jenkins and Wanner, 2014).

Aeration is an important piece of conventional wastewater treatment because it is an integral part of the AS process. This operation is essential for two different reasons. On the one hand, it is responsible for oxygen supply, which is essential for the metabolism of aerobic bacteria (Teixeira and Fonseca, 2006). On the other hand, it contributes for the spreading of dissolved oxygen (DO) throughout the aeration tank, thus increasing process effectiveness (Amaral et al., 2018). Moreover, aeration is reported as the operation that accounts for most of the energy consumption in wastewater treatment plants (Fayolle et al., 2007; Jiang et al., 2017; Rosso and Stenstrom, 2006), representing up to 70 per cent of the total energy expenditure (Fayolle et al., 2007). Therefore, the study of this operation is of the utmost importance to reduce operation costs and energy usage (Fayolle et al., 2007; Karpinska

and Bridgeman, 2016).

Amaral et al. (2017) argues that, to solve the problem associated with aeration, mathematical modelling of the entire aeration system is needed. The development of such models is essential in view of the design, optimisation, and control of wastewater treatment plants. Due to complexity of this task, the authors propose that the aeration system is divided into two different parts: air generation and distribution and oxygen transfer. This strategy allows to tackle the problem by studying parts of this system rather than studying the whole at once. Such an approach results in an increased understanding of the underlying mechanisms and the improvement of the predictive capabilities of the models (Amaral et al., 2017). The work performed in this thesis can be situated in the context of the second subdivsion: modelling of oxygen transfer.

The state-of-the-art modelling approaches for oxygen transfer are based on the gas-liquid mass transfer theory. This theory allows for the evaluation of the oxygen transfer rate (OTR) via the overall volumetric oxygen transfer coefficient, K_La. This parameter is the product of two different variables, K_L and a (Metcalf and Eddy, 2003). The former is the overall mass transfer coefficient and the latter is the interfacial area available for mass transfer per unit volume. K_La is often experimentally determined in a lumped form, due to difficulties in measuring the two parameters separately (Teixeira and Fonseca, 2006). The current modelling practice is simple and straightforward (Amaral et al., 2017, 2018): (1) determination of the K_La for water under standard conditions, following the American Society of Civil Engineers method (American Society of Civil Engineers, 1983); (2) estimation of the α-factor, i.e. the ratio between K_La for wastewater and water, experimentally or by adopting a value reported in the literature; (3) consideration of other effects on oxygen transfer, such as temperature, surfactant concentration, and fouling on diffused aerators; (4) calculation of the K_La under operating conditions; and (5) determination of the OTR.

Due to the high energy usage by the aeration system, it is easy to conclude that the current aeration modelling of oxygen transfer has much room for improvement (Pittoors et al., 2014). This is not surprising since the method used is too simplistic (Amaral et al., 2017). There are many different hydrodynamic and operating effects involved in oxygen transfer, such as the flow regime (Shah et al., 1982), the presence of surfactants (Rosso and Stenstrom, 2006; Jimenez et al., 2014), the rheological characteristics of AS (Ratkovich et al., 2013; Durán et al., 2016), the tank shape (Pittoors et al., 2014), the mixing conditions (Deckwer et al., 1974), the number and arrangement of diffusers (Gillot et al., 2005; Terashima et al., 2016), and the water depth (Gillot et al., 2005). Even though all these parameters significantly impact the oxygen transfer, only the α-factor is currently used to account for them (Amaral et al., 2017, 2018). Obviously, this makes this correction factor one of the most uncertain aeration parameters (Karpinska and Bridgeman, 2016), with reports stating that its value fluctuates through daily cycles and seasonal periods (Jiang et al., 2017). Despite this, the use of constant α-factors is still the most common practice in process design and modelling, which leads to nonoptimal designs (Jiang et al., 2017).

To improve oxygen transfer modelling, many researchers have been focusing on pinpointing the main physical mechanisms affecting this complex process. Shah et al. (1982), Terashima et al. (2016), and Sommer et al. (2017) identified bubble size distribution (BSD) as one of the key factors affecting oxygen transfer, since it affects both the gas holdup and the bubble size, which have effect on both K_L and a. Following the suggestion of these authors, Amaral et al. (2018) conducted a study in an aerated bubble column which aimed to create a new modelling strategy that explicitly involves the effect of BSD dynamics on oxygen transfer. During this study, the author varied both the viscosity of the liquid phase and the airflow rates, because these parameters significantly influence BSD dynamics. The development of this model lead the researchers to address the shortcomings in the body of knowledge of the oxygen transfer field. Therefore, this work is not only an important benchmark to comprehend the effects of BSD dynamics on oxygen transfer, but also a crucial starting point for more accurate and complete oxygen transfer modelling approaches.

The aim of this dissertation is to continue the work of Amaral et al. (2018) by developing a model that is able to predict the BSD dynamics observed by this author. The secondary objective is the clarification of the mathematical and physical background associated with BSD.

2. Background

The PBM framework is a mathematical scheme that tracks the number of entities - solid particles, bubbles or droplets - present within a system, considering their development and interactions with themselves as well as with the continuous phase (Yeoh et al., 2014). According to Nopens (2005), many of the processes involved in wastewater treatment deal with a distribution of properties under transient conditions, such as bubble size. Since PBM can describe the dynamics of properties that are characterised by distributions, the application of

this modelling approach was crucial for the success of this work. Moreover, Amaral et al. (2018) identified bubble coalescence as the phenomenon that dictates BSD dynamics in the analysed experimental set-up. Coalescence refers to the creation of a new bubble resulting from the collision of two or more distinct bubbles. Therefore, the description of this phenomenon and its association to the PBM framework was considered as a crucial component of this work.

2.1. The PBM framework

The general PBM Equation (PBME) is denoted by equation (1) (Ramkrishna, 2000):

$$\frac{\partial}{\partial t} f_1 + \nabla_{\mathrm{x}} \cdot \dot{X} f_1 + \nabla_{\mathrm{r}} \cdot \dot{R} f_1 = h \tag{1}$$

The first term on the left-hand side of equation (1) characterises the local change of the particle number density with time (i.e. the accumulation term). The second term represents the change of the number density due to advection in the external coordinates (physical space), while the third term denotes the change of the number density due to advection in internal coordinates (particle property space), indicating several particle growth phenomena. These two terms correspond to continuous processes. The term on the right-hand side of equation (3.1) is the net rate of generation of particles and represents discrete processes, such as coalescence (Ramkrishna, 2000; Nopens, 2005; Yeoh et al., 2014). The PBME must be supplemented with an initial and boundary conditions.

2.2. Bubble coalescence

The models developed to mathematically describe coalescence, so that the right-hand side of equation (1) can be closed are named coalescence kernels. The objective of these models is to calculate the coalescence frequency, i.e. the number of coalescence events per unit time. To determine this parameter, two terms need to be calculated: (1) the collision frequency, which denotes the number of collisions per unit time and (2) the coalescence efficiency, which determines the percentage of collisions that result in coalescence (Liao and Lucas, 2010). The kernel studied in this dissertation was proposed by Prince and Blanch (1990). This model is summarised by equation (2).

$$\Gamma_{j,k} = \theta_{j,k} \times \lambda_{j,k} \tag{2}$$

In equation (2), $\Gamma_{j,k}$ is the coalescence frequency, $\theta_{j,k}$ is the collision frequency, and $\lambda_{j,k}$ is the coalescence efficiency.

2.2.1 Collision frequency

The mathematical expression developed by Prince and Blanch (1990) considers three different sources of collision, assumed to be additive: (1) turbulence, (2) buoyancy, and (3) laminar shear. The last one is not explained as it was considered that collisions due to laminar shear did not take place. The reason for this is that the studied bubble column always operated at superficial gas velocities inferior to 5 cm/s (Amaral et al., 2018). According to Prince and Blanch (1990), collisions due to this mechanism only occur at velocities superior to this threshold.

The turbulent collision rate is illustrated by equation (3):

$$\theta^T_{j,k} = C_1^{'} (d_j + d_k)^2 (d_j^{2/3} + d_k^{2/3})^{1/2} \varepsilon^{1/3} \tag{3}$$

In equation (3), $\theta^T_{j,k}$ represents the turbulent collision rate of bubbles j and k, $C_1^{'}$ is a correcting parameter, d_j and d_k are the diameters of the bubbles involved in the collision, and ε is the turbulent energy dissipation rate, which can be determined by equation (4).

$$\varepsilon = \frac{Qg}{\pi R_T^2} \frac{P_2 \, ln(P_1/P_2)}{P_1 - P_2} \tag{4}$$

In equation (4), Q is the volumetric gas flow rate, g is the acceleration of gravity, R_T is radius of the bubble column, and P_1, P_2 are the pressures at the bottom and top of the column, respectively.

The collisions resulting from buoyancy are calculated with the expression presented in equation (5).

$$\theta^B_{j,k} = S_{j,k} \, |u_{r,j} - u_{r,k}| \tag{5}$$

In equation (5), $\theta^B_{j,k}$ denotes the buoyancy-driven collision rate of bubbles j and k, $S_{j,k}$ is the collision cross-sectional area which depends on the diameters of bubbles j and k, and $u_{r,j}$ and $u_{r,k}$ are the rising velocities of bubbles j and k.

Since the mechanisms are assumed to be additive, the expression that calculates the total collision frequency, $\theta_{j,k}$, is illustrated by equation (6).

$$\theta_{j,k} = \theta^T_{j,k} + \theta^B_{j,k} \tag{6}$$

2.2.2 Coalescence efficiency

The coalescence efficiency expression is a function of the drainage, rupture, and contact times. The first is associated with the time required for the film trapped between the two bubbles to drain. The second is related to the time needed for the liquid

film to rupture. The sum of these two times is the coalescence time and represents the time required for the bubbles to merge. The third corresponds to the time they are close enough for coalescence to take place. The probability of a collision resulting in coalescence relies on the relationship between the coalescence and contact times. The coalescence efficiency expression (equation (7)) can be deduced in two steps. In the first, the coalescence and contact times are assumed to be random variables and the coalescence time to be normally distributed. In the second, the expression for the probability of coalescence based on the normal distribution is simplified by assuming that the standard deviation for the coalescence time is zero, i.e. the coalescence time is not distributed (Tsouris and Tavlarides, 1994). This leads to the following equation.

$$\lambda_{j,k} = exp(-\frac{t_{j,k}}{\tau_{j,k}}) \tag{7}$$

In equation (7), $\lambda_{j,k}$ represents the coalescence efficiency, $t_{j,k}$ the time required for coalescence of bubbles of radius r_j and r_k, which is given by equation (8). The contact time between bubbles j and k, $\tau_{j,k}$, can be evaluated with equation (9).

$$t_{j,k} = (\frac{r_{j,k}^3\,\rho_L}{16\,\sigma_L})^{1/2}\,ln\frac{h_0}{h_f} \tag{8}$$

In equation (7), h_0 is the initial film thickness, h_f the critical film thickness, and $r_{j,k}$ the equivalent radius of bubbles j and k. According to Liao and Lucas (2010), h_0 and h_f usually take the values of $10^{-4}\,m$ and $10^{-8}\,m$, respectively.

It is important to note that equation (8) can only be derived if these assumptions are considered: (1) the rupture time is neglected, because the concentration of surfactant species is equal to zero; (2) the gas-liquid interface is mobile; (3) the Hamacker constant, which accounts for the mutual attraction of molecules on opposite sides of the liquid film, is disregarded; (4) the effect of bubble deformation by turbulent eddies is not considered; and (5) the radius of the liquid disk between coalescing bubbles is the bubble radius. On the other hand, equation (9) is derived solely from dimensional considerations and can only be regarded as an order of magnitude approximation (Prince and Blanch, 1990). It should be noted that the characteristic length, $r_{j,k}$, is considered to be arbitrary.

$$\tau_{j,k} = \frac{r_{j,k}^{2/3}}{\varepsilon^{1/3}} \tag{9}$$

3. Implementation

The implementation is divided into three sections: (1) solution method (SM); (2) modifications made to the coalescence kernel proposed by Prince and Blanch (1990); and (3) insertion of the kernel into the PBME. Due to the inherent complexity of PBMEs, analytical solutions to these equations can only be found in idealised situations or simplified cases. Therefore, the successful use of PBMEs relies on numerical methods (Kumar and Ramkrishna, 1996). In this work, the SM implemented was the Fixed Pivot Technique (FPT). The coalescence kernel developed by Prince and Blanch (1990) has been reported to overestimate the coalescence frequency (Bhole et al., 2008; Chen et al., 2005; Van Den Hengel et al., 2005). This over-prediction is mainly associated with the coalescence efficiency term, thus modifications were made to this parameter. Finally, the coupling strategy implemented to guarantee consistency between the PBM framework and the developed coalescence kernel is explained.

3.1. The Fixed Pivot Technique

The FPT is a numerical SM, developed by Kumar and Ramkrishna (1996), which relies on the discretisation of the PBME. To achieve this, the entire size range was divided into small sections. The authors defined two types of points in this space: (1) points which limit a section, v_i and v_{i+1} and (2) points within a section that represent the sections particle population, x_i, such that $v_i < x_i < v_{i+1}$. The sections contained between the points v_i and v_{i+1} are named the ith bin and the points x_i are called pivots. Next, a discrete set of equations that describe the redistribution of particles whose sizes differ from the pivotal sizes (x_i) was derived. It is worth noting that these equations assure the preservation of two moments. The FPT expression is presented in equation (10):

$$\frac{dN_i}{dt} = \sum_{\substack{j,k \\ x_{i-1}\leqslant(x_j+x_k)\leqslant x_{i+1}}}^{j\geqslant k} (1-\frac{1}{2}\,\delta_{j,k})\,\eta\,\Gamma_{j,k}\,N_j\,N_k - N_i\sum_{k=1}^{M}\Gamma_{i,k}\,N_j \tag{10}$$

The first term represents the birth and the second one the death due to the coalescence process. N_i denotes the number concentration of particles in bin i and $\Gamma_{j,k}$ represents the coalescence frequency for sizes x_j, x_k. The remaining parameters are $\delta_{j,k}$ and η. The former is the Kronecker delta function, which assumes the value 0 when $x_j \neq x_k$ and 1 when $x_j = x_k$ (avoids counting coalescence events between bubble pairs twice). The latter - defined in equation (11) - guarantees the preservation of moments 0 (numbers) and 1 (mass). It should be noted that equation (10) can only be derived if one

assumes perfectly mixed conditions and no bubble growth.

$$\eta = \begin{cases} \frac{x_{i+1}-v}{x_{i+1}-x_i} & x_i \leq v \leq x_{i+1} \\ \frac{v-x_{i-1]}}{x_i-x_{i-1}} & x_{i-1} \leq v \leq x_i \end{cases} \quad (11)$$

3.2. Modifications to the coalescence kernel

Considering the findings of Van Den Hengel et al. (2005) and Chen et al. (2005), it was decided to decompose the coalescence time into drainage time and rupture time and discard the contact time expression proposed by Prince and Blanch (1990). This allows the model to cope with the influence of the conditions of the gas-liquid interface, such as mobility, molecular interactions, and surfactant concentration, on the coalescence efficiency (Lee et al., 1987). Moreover, it strongly influences the size dependent part of coalescence efficiency, as the critical film thickness, which is highly affected by bubble size, is usually assumed to be a constant (Lee et al., 1987). When the rupture time is considered, the coalescence time increases, leading to a decrease of the coalescence efficiency. Therefore, the over-prediction associated with the model developed by Prince and Blanch (1990) is mitigated. The kernel used in this dissertation is denoted in equation (12):

$$\Gamma_{j,k} = (\theta^T_{j,k} + \theta^B_{j,k}) \times exp(-\frac{t_{d\,j,k} + t_{r\,j,k}}{t_{c\,j,k}}) \quad (12)$$

To determine the drainage time $t_{d\,j,k}$, the expression used was the one developed by Prince and Blanch (1990) (equation (3.15)). The rupture time, $t_{r\,j,k}$, and contact time, $t_{c\,j,k}$, were determined by model calibration. It is worth noting that the factors involved in these mathematical equations were found to be unknown. On the one hand, the influence of the conditions of the interface on coalescence efficiency was out of the scope of the experimental work performed by Amaral et al. (2018), thus the information needed to model this influence was not available. On the other hand, the expression that describes the contact time was deduced solely by dimensional analysis and it is only an approximation of the order of magnitude.

3.3. Insertion of the coalescence kernel into the PBME

To couple equations (10) and (12), the coalescence frequency was divided by the volume of the bubble created in the coalescence event and multiplied by the volume of the fluid where the coalescence process is taking place. The former operation transforms the volume of bubbles coalescing per unit time in a unit volume into the number of coalescence events per unit time occurring in a unit volume. The latter produces the number of coalescence events per unit time taking place in the volume considered. These considerations allow the resulting coalescence frequency, denoted by equation (13), to be consistent with equation (10):

$$\Gamma_{j,k} = V_{section} \times \frac{((\theta^T_{j,k} + \theta^B_{j,k}) \times \lambda_{j,k})}{(v_j + v_k)} \quad (13)$$

Equations (10) and (13) represent the model developed to predict BSD dynamics. These equations were implemented in MATLAB® and solved with the classical Runge-Kutta method.

4. Results and discussion

The model developed was applied to the bubble column studied by Amaral et al. (2018). The author used three different solutions: tap water (CW) and xanthan gum (XG) solutions at concentrations of 0.2 (XG0.2) and 0.8 (XG0.8) kg/m^3. The use of XG solutions allows to mimic the viscosity of AS, which is an important parameter to account for in BSD. Moreover, four airflow rates were tested: 2, 4, 6, and 8 L/min. To study the evolution of BSD, the bubble column was divided into seven sections: 5, 20, 40, 60, 80, 100, and 120 cm from the diffuser. The author measured the experimental BSD for each solution and AR along the height of the system, thus seven BSDs were derived for each solution and airflow rate. The BSD measured at 5 cm was used as the initial condition supplemented to equation (10). To calibrate the model, a sum of squared errors (SSE) function was minimised. Only the BSD measured at 120 cm was considered. The remaining measurements were used to validate the model, as they describe the evolution of BSD dynamics.

4.1. Model calibration

Due to the high number of operating conditions studied, only the results for airflow rates of 2 and 8 L/min are presented. The results for CW, XG0.2, and XG0.8 are displayed in Figures 1, 2, and 3, respectively.

The effect of airflow rate on BSD in CW can be studied by comparing the experimental distributions. After analysing Figure 1, one can observe a shift to larger bubbles at a higher airflow rate. An increased airflow rate enables a larger volume of gas to enter the system, which translates into a higher gas holdup value. This raises the number of bubbles and introduces more turbulence, which in turn increases collision between bubbles, making successful coalescence events more likely to occur. Since the reason for growth along the height of the column is coalescence, it follows that bubbles grow more at increased airflow rates. In a similar way,

Figure 2 depicts a shift to larger bubbles at a higher airflow rate. This was expected, since the rationale presented to justify this behaviour in CW also holds for XG0.2.

In Figure 3, the shift to larger bubbles is not clear. In fact, measurements show that bubbles do not grow along the height of the column at an airflow rate of 8 L/min. As stated by Amaral et al. (2018), the reason for this observation is unclear, as it was expected that bubbles would grow along the height of the column due to coalescence.

The effect of liquid viscosity on BSD can also be assessed through the analysis of Figures 1 and 2. The comparison of the measured BSDs leads to one conclusion: a higher liquid viscosity reduces growth along the height of the column. By analysing the grey dotted lines in Figures 1 and 2, it is possible to observe that the shift to larger bubbles is less pronounced in XG0.2. As previously stated, bubbles grow along the height of the column due to coalescence, which is more prevalent when the number of collisions increases. If the liquid is more viscous, the movement of bubbles through the fluid is impaired. Hence, the number of collisions diminishes, leading to fewer coalescence events. Once again, this behaviour is not clear in Figure 3.

The sum of squared errors (SSE) enables the evaluation of the calibration process, since its value quantifies the fit between experimental and calibration results. When the value of SSE approaches zero, the calibration and experimental curves overlap, and thus the model is adequately calibrated. The values determined in the calibration process for each solution and airflow rate are summarised in Table 1.

The calibration process produced better results for CW and XG0.2 than for XG0.8. Two observations support this conclusion: (1) the SSE values presented in Table 1 for CW and XG0.2 are considerably lower than those determined for XG0.8 and (2) the calibrated BSD curve (black lines) and experimental BSD curve at 120 cm from diffuser (grey dotted lines) are similar for CW and XG0.2, whereas for XG0.8 they are different. The discrepancies observed are related to the experimental process and model.

Table 1: Values of SSE obtained in the calibration process for each solution and airflow rate (AR).

Solution	AR [L/min]	SSE
CW	2	45
	8	22
XG0.2	2	143
	8	60
XG0.8	2	682
	8	529

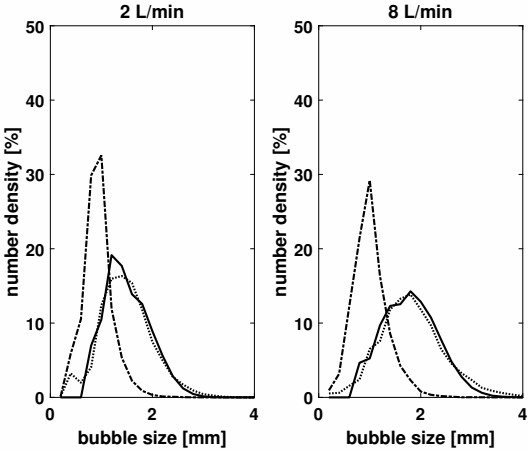

Figure 1: Experimental BSD for CW (grey dash-dot line - at 5 cm from diffuser; grey dotted line - at 120 cm from diffuser) and calibrated BSD (black line - at 120 cm from diffuser).

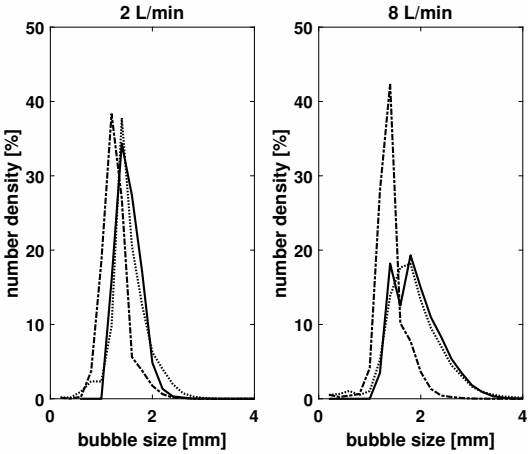

Figure 2: Experimental BSD for XG0.2 (grey dash-dot line - at 5 cm from diffuser; grey dotted line - at 120 cm from diffuser) and calibrated BSD (black line - at 120 cm from diffuser).

A plausible justification for the observations made for XG0.8 is associated with the experimental procedure. As previously stated, Amaral et al. (2018) observed an unexpected behaviour for XG0.8 8 L/min. Although the author did not provide an explicit justification, it mentioned that further research would be conducted to explain this observation. Helser (2018) repeated the experiment performed for XG0.8 two more times. This decision arose from the fact that, in the specific case of XG0.8, the solution becomes opaque, hindering the identification of the bubbles by the digital image analysis used. It should be noted that the experimental procedure is the one described in Amaral et al. (2018). The calibration results obtained were similar to one another and are depicted in Figure 4.

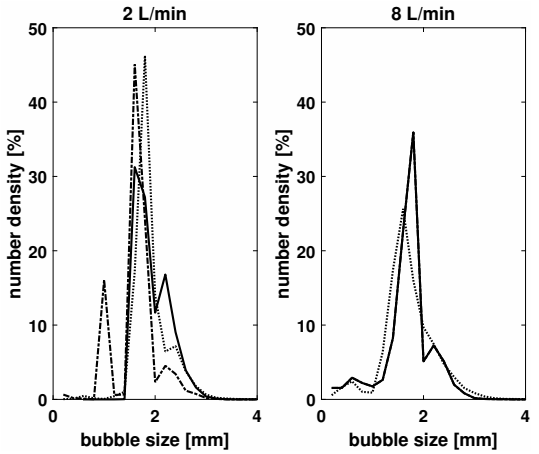

Figure 3: Experimental BSD for XG0.8 obtained in the two repeated experiments (grey dash-dot line - at 5 cm from diffuser; grey dotted line - at 120 cm from diffuser) and calibrated BSD (black line - at 120 cm from diffuser).

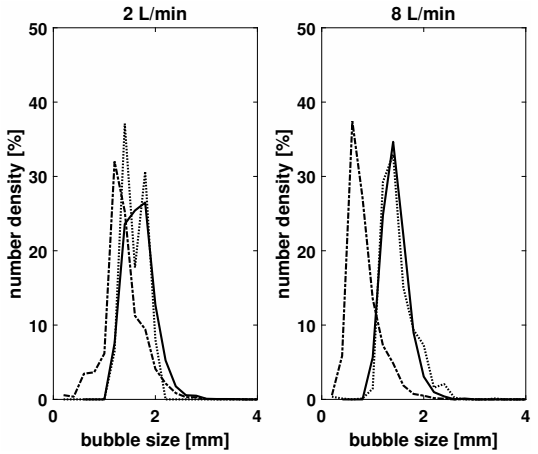

Figure 4: Experimental BSD for XG0.8* (grey dash-dot line - at 5 cm from diffuser; grey dotted line - at 120 cm from diffuser) and calibrated BSD (black line - at 120 cm from diffuser).

In Table 2, the SSE is presented. To distinguish the repeated experiments, the solution is referred to as XG0.8*.

Table 2: Values of SSE obtained in the calibration process for the repeated experiments in XG0.8*.

Solution	AR [L/min]	SSE
XG0.8*	2	302
	8	109

In this case, the curves are similar and the SSE values are significantly lower than the ones determined for XG0.8 presented in Table 2. This leads to the conclusion that experimental error is a significant contributor for the misfit between model and experimental results. The results considered henceforth are the ones presented in Figure 4 and denoted by XG0.8*.

The model developed can also contribute for the discrepancies between model and experimental results. As previously stated, the model formulated is a modification of the expression proposed by Prince and Blanch (1990). The modifications made to the original model are mainly associated with the coalescence efficiency term, since it has been reported that this term is the cause for the over-prediction associated with the model of these authors (Chen et al., 2005; Van Den Hengel et al., 2005; Laakkonen et al., 2007; Bhole et al., 2008). According to the experimental observations, the effect of liquid viscosity is crucial because it strongly influences the amount of collisions, thus affecting the coalescence phenomenon. Hence, the effect of liquid viscosity on the collision frequency term should be explicitly considered. However, to the author's best knowledge, no turbulent collision rate expression considering this influence has been implemented in coalescence kernels reported in the literature. Furthermore, Lee et al. (1987) argues that viscosity should also affect the drainage time because, in viscous liquids, the film surfaces become partially immobile which greatly increases the value of this parameter.

Although the model does not directly consider the effect of viscosity on both turbulent collision rate and drainage time, the modifications made to the model developed by Prince and Blanch (1990) enable it to account for them. This is proven by the results shown in Figures 1, 2, and 4 since the model can describe BSD in all the solutions studied. The parameters that are considering the influence of liquid viscosity on BSD are the rupture and contact times, because they were used to calibrate the model. Hence, the errors caused by changes in liquid viscosity are compensated by the combination of values found in the calibration process. The drawback of this strategy is that calibrated parameters tend to lose their physical meaning, since the influence of numerous effects are encompassed in their values. To evaluate the quality of this modelling approach, the analysis of the values of rupture and contact times for all conditions are presented in Table 3.

In the case of CW, the calibrated values for rupture and contact times are expected to be almost identical to the ones of the actual physical parameters, since the considerations used to develop equations (2) and (7) hold true. The values obtained for the XG solutions can be compared to these ones to assess their veracity. Although the effect of viscosity was not properly addressed in the turbulent collision frequency and drainage time, the computed

Table 3: Values of t_r and t_c determined by the calibration process for each solution and airflow rate (AR).

Solution	AR [L/min]	t_r [$\times 10^{-3}$ s]	t_c [$\times 10^{-3}$ s]
CW	2	27	2.1
	4	38	2.9
	6	78	5.6
	8	79	5.6
XG0.2	2	1.8	0.23
	4	4.2	0.40
	6	35	2.6
	8	57	4.2
XG0.8*	2	1.4	0.20
	4	1.7	0.21
	6	2.0	0.20
	8	2.2	0.20

parameters for XG solutions are close to the order of magnitude of the ones calculated for CW. This proves that the parameters used for calibration allow the model to cope with the errors introduced by the assumptions, without significantly jeopardising their physical interpretation.

Considering the previous discussion, it can be concluded that the model is then able to cope with changes in liquid viscosity, which can be seen in Figures 1, 2, and 4. Nonetheless, the effect of liquid viscosity should be explicitly considered. In fact, the dissimilarities between the curves increases for XG0.8*, showing that model predictions are less accurate for more viscous solutions. Since the influence of this parameter was not completely described, the misfit between model and experimental results can be partially related to the model formulated.

4.2. Model validation

Due to the high number of experimental measurements, only the data for 20, 60, and 100 cm are shown.

4.2.1 CW and XG0.2 results

The validation results for CW and XG.2 are presented in Figure 5 and 6, respectively.

By analysing Figures 5 and 6, it is possible to conclude that the model can predict BSD dynamics in CW and XG0.2.

4.2.2 XG0.8* results

The validation results for XG0.8* are illustrated in Figure 7.

When looking at the experimental results measured at 2 L/min, one can observe that the growth along the height of the column is almost inexistent.

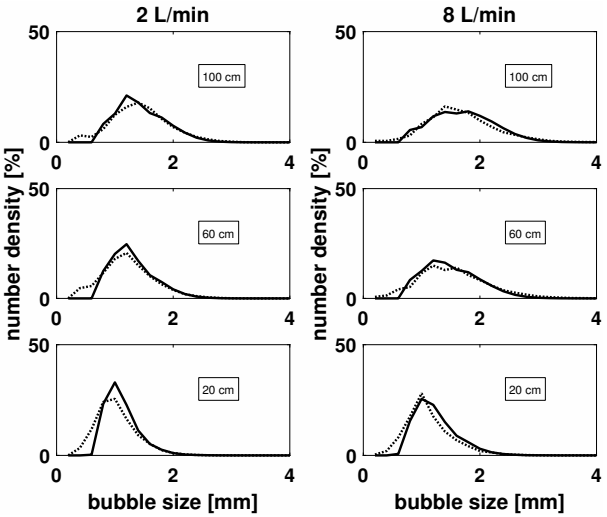

Figure 5: Experimental BSD for CW (grey dotted line) and BSD predicted by the model (black line).

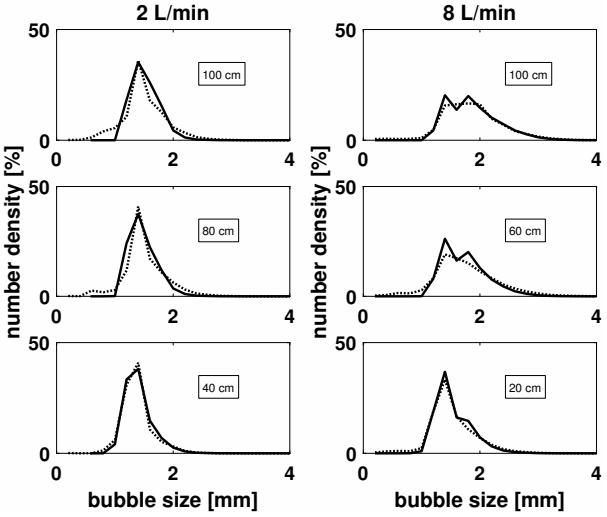

Figure 6: Experimental BSD for XG0.2 (grey dotted line) and BSD predicted by the model (black line).

On the one hand, the misfit between model and experimental results can be related to the corruption of experimental data. As previously stated, the BSDs measured in XG0.8 by Amaral et al. (2018) (see Figure 3) showed an unexpected behaviour and, as such, were discarded. Although the results depicted in Figure 6 do not show the same trends, it is possible to verify that the growth of bubbles is not concordant with the one observed in CW and XG0.2. On the other hand, the fact that the influence of liquid viscosity was not explicitly modelled introduces errors in the model, making it lose part of its predictive capability for more viscous solutions. In addition, the influence of conditions of the interface can also be affecting model predictions.

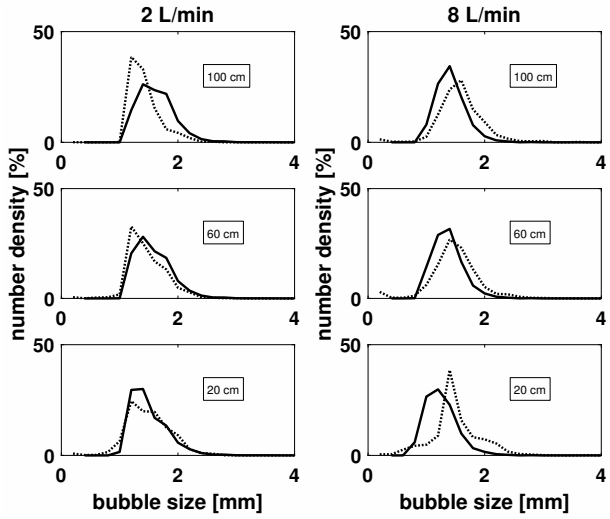

Figure 7: Experimental BSD for XG0.8* (grey dotted line) and BSD predicted by the model (black line).

Therefore, the discrepancies observed can be associated with experimental data corruption and model formulation. Even though the disparity between model and experimental results is more pronounced in XG0.8*, the model has an adequate performance.

In conclusion, the model can predict BSD dynamics in every case.

5. Conclusions

The BSD dynamics observed by Amaral et al. (2018) were successfully described using the PBM framework in conjunction with a coalescence model. The formulation of the developed model produced valuable insights on the limitations of current coalescence modelling approaches. The coalescence models reported in the literature lack robustness and do not consider numerous effects on BSD, which were identified as key to correctly describe the phenomenon. The impact of critical film thickness on coalescence time should not be ignored, as this parameter strongly depends on bubble size and conditions of the interface. Moreover, the determination of a contact time based on dimensional analysis should be avoided.

According to the experimental data collected by Amaral et al. (2018), viscosity has a significant impact on the turbulent collision rate. This effect was considered implicitly by the modelling strategy developed in this work. However, a need to account for this variable explicitly was identified. For this reason, future research should focus on this area so that coalescence models can be refined.

A novel mathematical approach to predict BSD dynamics due to coalescence was proposed. The model was validated for the system studied by Amaral et al. (2018) and produced very good results, proving that it can be a powerful tool in predicting BSD dynamics. The implementation of this modelling approach in state-of-the-art oxygen transfer modelling can be the first step to improve the prediction of $K_L a$, in turn, optimising the estimation of OTR in wastewater treatment. Therefore, this model can be a solution to the challenges imposed by high energy usages associated with aeration, leading to the mitigation of the environmental impact and an increase in cost-effectiveness of wastewater treatment plants.

References

Amaral, A.; Schraa, O.; Rieger, L.; Gillot, S.; Fayolle, Y.; Bellandi, G.; Amerlinck, Y.; Mortier, S. T.; Gori, R.; Neves, R., and Nopens, I. Towards advanced aeration modelling: From blower to bubbles to bulk. *Water Science and Technology*, 75(3):507–517, 2017.

Amaral, A.; Bellandi, G.; Rehman, U.; Neves, R.; Amerlinck, Y., and Nopens, I. Towards improved accuracy in modeling aeration efficiency through understanding bubble size distribution dynamics. *Water Research*, 131:346–355, 2018.

American Society of Civil Engineers. Development of standard procedures for evaluating oxygen transfer devices, 1983.

Bhole, M.; Joshi, J., and Ramkrishna, D. CFD simulation of bubble columns incorporating population balance modeling. *Chemical Engineering Science*, 63(8):2267–2282, 2008.

Chen, P.; Sanyal, J., and Duduković, M. P. Numerical simulation of bubble columns flows: Effect of different breakup and coalescence closures. *Chemical Engineering Science*, 60(4):1085–1101, 2005.

Deckwer, W. D.; Burckhart, R., and Zoll, G. Mixing and mass transfer in tall bubble columns. *Chemical Engineering Science*, 29(11):2177–2188, 1974.

Durán, C.; Fayolle, Y.; Pechaud, Y.; Cockx, A., and Gillot, S. Impact of suspended solids on the activated sludge non-newtonian behaviour and on oxygen transfer in a bubble column. *Chemical Engineering Science*, 141:154–165, 2016.

Fayolle, Y.; Cockx, A.; Gillot, S.; Roustan, M., and Héduit, A. Oxygen transfer prediction in aeration tanks using CFD. *Chemical Engineering Science*, 62(24):7163–7171, 2007.

Gillot, S.; Capela-Marsal, S.; Roustan, M., and Héduit, A. Predicting oxygen transfer of fine bubble diffused aeration systems - Model issued

from dimensional analysis. *Water Research*, 39 (7):1379–1387, 2005.

Helser, J. *Monitoring, data analysis and modelling of gas-liquid mass transfer in wastewater treatment*. Master's thesis, Ghent University, 2018.

Jenkins, D. and Wanner, J. *100 Activated Sludge - 100 years and counting*. IWA Publishing, 2014.

Jiang, L. M.; Garrido-Baserba, M.; Nolasco, D.; Al-Omari, A.; DeClippeleir, H.; Murthy, S., and Rosso, D. Modelling oxygen transfer using dynamic alpha factors. *Water Research*, 124:139–148, 2017.

Jimenez, M.; Dietrich, N.; Grace, J. R., and Hébrard, G. Oxygen mass transfer and hydrodynamic behaviour in wastewater: Determination of local impact of surfactants by visualization techniques. *Water Research*, 58:111–121, 2014.

Karpinska, A. M. and Bridgeman, J. CFD-aided modelling of activated sludge systems - A critical review. *Water Research*, 88:861–879, 2016.

Kumar, S. and Ramkrishna, D. On the solution of population balance equations by discretizationI. A fixed pivot technique. *Chemical Engineering Science*, 51(8):1311–1332, 1996.

Laakkonen, M.; Moilanen, P.; Alopaeus, V., and Aittamaa, J. Modelling local bubble size distributions in agitated vessels. *Chemical Engineering Science*, 62(3):721–740, 2007.

Lee, C.-H.; Erickson, L., and Glasgow, L. Bubble breakup and coalescence in turbulent gas-liquid dispersions. *Chemical Engineering Communications*, 59(1-6):65–84, 1987.

Liao, Y. and Lucas, D. A literature review on mechanisms and models for the coalescence process of fluid particles. *Chemical Engineering Science*, 65 (10):2851–2864, 2010.

Maitland, P. *Biology of fresh waters*. Chapman and Hall, 1990.

Metcalf and Eddy. *Wastewater engineering treatment and reuse*. McGraw-Hill, 2003.

Mihelcic, J. R. and Zimmerman, J. B. *Environmental engineering fundamentals, sustainability, design*. John Wiley & Sons, Inc., 2010.

Nopens, I. *Modelling the activated sludge flocculation process: A population balance approach*. PhD thesis, Ghent University, 2005.

Pittoors, E.; Guo, Y., and Van Hulle, S. W. Modeling dissolved oxygen concentration for optimizing aeration systems and reducing oxygen consumption in activated sludge processes: A review. *Chemical Engineering Communications*, 201(8): 983–1002, 2014.

Prince, M. J. and Blanch, H. W. Bubble coalescence and breakup in air sparged bubble columns. *AIChE Journal*, 36(10):1485–1499, 1990.

Ramkrishna, D. *Population balances theory and applicatons to particulate systems in engineering*. Academic Press, 2000.

Ratkovich, N.; Horn, W.; Helmus, F. P.; Rosenberger, S.; Naessens, W.; Nopens, I., and Bentzen, T. R. Activated sludge rheology: A critical review on data collection and modelling. *Water Research*, 47(2):463–482, 2013.

Rosso, D. and Stenstrom, M. K. Surfactant effects on α-factors in aeration systems. *Water Research*, 40(7):1397–1404, 2006.

Shah, Y. T.; Kelkar, B. G.; Godbole, S. P., and Deckwer, W. D. Design parameters estimations for bubble column reactors. *AIChE Journal*, 28 (3):353–379, 1982.

Sommer, A. E.; Wagner, M.; Reinecke, S. F.; Bieberle, M.; Barthel, F., and Hampel, U. Analysis of activated sludge aerated by membrane and monolithic spargers with ultrafast X-ray tomography. *Flow Measurement and Instrumentation*, 53:18–27, 2017.

Teixeira, J. A. and Fonseca, M. M. *Reatores biológicos*. Lidel, 2006.

Terashima, M.; So, M.; Goel, R., and Yasui, H. Determination of diffuser bubble size in computational fluid dynamics models to predict oxygen transfer in spiral roll aeration tanks. *Journal of Water Process Engineering*, 12:120–126, 2016.

Tsouris, C. and Tavlarides, L. L. Breakage and coalescence models for drops in turbulent dispersions. *AIChE Journal*, 40(3):395–406, 1994.

Van Den Hengel, E. I.; Deen, N. G., and Kuipers, J. A. Application of coalescence and breakup models in a discrete bubble model for bubble columns. *Industrial and Engineering Chemistry Research*, 44(14):5233–5245, 2005.

Yeoh, G. H.; Cheung, C. P., and Tu, J. *Multiphase flow analysis using population balance modeling*. Elsevier, 2014.